

LINEAR DYNAMICS OF LARGE-SCALE STRUCTURES IN TURBULENT JETS

Oliver T. Schmidt

Dept of Mechanical and Civil Engineering
California Institute of Technology
1200 E. California Boulevard
Pasadena, CA 91125-2100
oschmidt@caltech.edu

Tim Colonius

Dept of Mechanical and Civil Engineering
California Institute of Technology
1200 E. California Boulevard
Pasadena, CA 91125-2100
colonius@caltech.edu

Guillaume A. Brès

Cascade Technologies, Inc.
2445 Faber Pl., Suite 100
Palo Alto, CA 94303-3347
gbres@cascadetechnologies.com

ABSTRACT

Large-scale coherent structures are educed from a large eddy simulation of an initially turbulent, $M = 0.9$ isothermal jet by means of spectral proper orthogonal decomposition. The modal energy spectra reveal a low-rank behavior that leads to a preferred amplification of Kelvin-Helmholtz-type wavepackets within certain frequency bands. We investigate the linear frequency response of the turbulent mean flow, and demonstrate that a resolvent analysis is capable of predicting the jet’s statistical low-rank behavior, and the associated modal structures accurately. The results also explain why previous wavepacket models based on the parabolized stability equations were largely successful in predicting modal shapes for certain frequencies, but not at others.

INTRODUCTION

Large-scale coherent structures in turbulent jets have been studied extensively since their early experimental observation by Mollo-Christensen (1963). Crighton & Gaster (1976) were among the first to interpret these coherent structures as modal perturbations about the temporal mean flow. Based on a separation-of-scales argument, the mean flow can be regarded as a base state which can be analyzed by means of linear stability theory. Large-scale structures in jets are of particular engineering interest as they are intimately linked to the dominant low aft-angle (with respect to the jet axis) noise, for example of jet engines. Their role as compact acoustic sources of sound is well established through a large body of theoretical and experimental studies (Jordan & Colonius, 2013).

We investigate the optimally forced linear dynamics of the turbulent mean of an isothermal subsonic turbulent jet issued from a convergent-straight nozzle. Modal solutions are obtained by means of global resolvent analysis, and the results are compared to large-scale coherent structures educed from a large eddy simulation (LES) database via spectral proper orthogonal decomposition (SPOD). In

Towne *et al.* (2016b) and Schmidt *et al.* (2016b), we showed that high subsonic jets exhibit *intrinsic* dynamics in the form of acoustic resonance between the nozzle and a frequency-dependent downstream location within the potential core. Here, we are interested in the jet’s *extrinsic* linear dynamics, and more specifically, its response to optimal forcing.

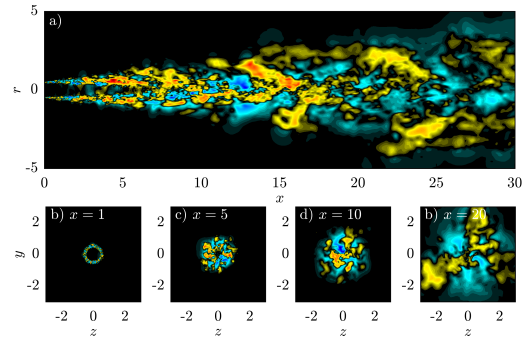


Figure 1. Instantaneous streamwise perturbation velocity field of the turbulent jet LES.

LARGE EDDY SIMULATION DATABASE

Large-scale coherent structures are educed from 10,000 snapshots of a large eddy simulation of a $M_j = 0.9$, $Re \approx 10^6$, isothermal, turbulent jet. Figure 1 shows an example of the instantaneous flow field. The database was calculated with the compressible flow solver “Charles” developed at Cascade Technologies (Brès *et al.*, 2017). We denote by $q(x, t) = [\rho \ u_x \ u_r \ u_\theta \ T]^T(x, r, \theta, t)$ the state vector of primitive variables. u_x , u_r , u_θ are the cylindrical velocity components, and ρ and T the density and temperature, respectively. All variables are non-dimensionalized by their centerline value in the nozzle plane and the nozzle diameter. The Strouhal number St is used to represent the

frequency in dimensionless form. The snapshots are separated by $\Delta t = 0.2$ dimensionless acoustic time units, and interpolated on a $656 \times 138 \times 128$ cylindrical grid spanning $x, r, \theta \in [0, 30] \times [0, 6] \times [0, 2\pi]$. The fluctuations q' about the long time mean \bar{q} are found from the usual Reynolds decomposition

$$q(x, r, \theta, t) = \bar{q}(x, r, \theta) + q'(x, r, \theta, t). \quad (1)$$

Under the assumption that the jet is statistically stationary, and since the jet is round, we further decompose the data into temporal and azimuthal modes as

$$q'(x, r, \theta, t) = \sum_{m, \omega} q_{m\omega}(x, r) e^{-i(\omega t - m\theta)}. \quad (2)$$

Energy is measured in terms of the inner product and its associated norm

$$\|q\|_E^2 = \langle q, q \rangle_E = q^H W q, \quad (3)$$

based on the weighting

$$\iiint q^H \text{diag} \left(\frac{\bar{T}}{\gamma \bar{\rho} M^2}, \bar{p}, \bar{p}, \bar{p}, \frac{\bar{p}}{\gamma(\gamma-1)\bar{T}M^2} \right) q r \, dx dr d\theta \quad (4)$$

for compressible flows. The quadrature weights and the weights for the individual state variables are absorbed into the weight matrix W in the discretized form above.

SPECTRAL PROPER ORTHOGONAL DECOMPOSITION

For comparison with linear theory, we seek a modal decomposition of the simulation data in the frequency domain. For non-periodic but statistically stationary data, such a decomposition can be found by a proper orthogonal decomposition (POD) of an ensemble of (assumably) independent Fourier realizations of the flow. To this end, we partitioning the database into sequences of 256 snapshots with an overlap of 50%. Each sequence is Fourier decomposed in time, leaving us with an ensemble $Q = [q_{m\omega}^{(1)} \quad q_{m\omega}^{(2)} \quad \dots \quad q_{m\omega}^{(N)}]$ of $N = 78$ Fourier realizations. For each frequency, the eigenvalue decomposition

$$Q^H W Q \Psi = \Psi \Lambda. \quad (5)$$

of the (weighted) cross-spectral density matrix $Q^H W Q$ yields a basis $\hat{Q} = Q \Psi$ of orthonormal modes which maximize the energy measured in the compressible energy norm (4). As in the resolvent analysis, we sort the eigenvalues such that $\hat{q}_{m\omega}^{(1)}$ is the most energetic mode. We term this decomposition spectral proper orthogonal decomposition (SPOD).

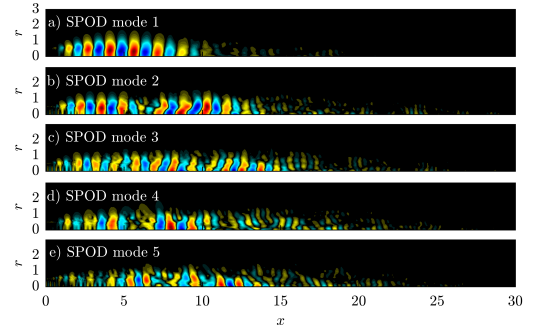


Figure 2. Normalized pressure field of the five most energetic SPOD modes for $St = 0.5$ and $m = 0$.

Figure 2 shows five most energetic SPOD modes for $St = 0.5$. The leading mode shown in figure 2(a) resembles a wavepacket similar to a Kelvin-Helmholtz (K-H) shear-layer instability. The second mode in figure 2(b) shows a double-wavepacket structure. Higher modes appear as increasingly less organized.

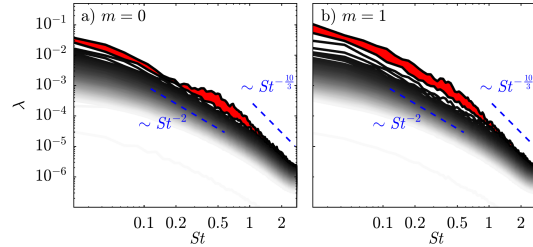


Figure 3. SPOD eigenvalues (\blacksquare , $\lambda_1 > \lambda_2 > \dots > \lambda_N$) as a function of frequency for $m = 0$ and $m = 1$. The difference between the leading and the second mode is highlighted in red (\blacksquare).

The SPOD eigenvalues shown in 3 are a direct measure of the modal energy. For both $m = 0$ and $m = 1$, an almost monotonic decrease of modal energy with frequency is observed. For frequencies larger than $St \gtrsim 1$, the modal energies presumably approach a slope of $-\frac{10}{3}$. Note that $St = 2.78$ is the highest frequency permitted by the saving interval of the database. A slope of -2 is shown for comparison with later results from the resolvent analysis. It is also observed that the difference between energy levels of subsequent modes is largest for the leading modes. This holds true for the first and second mode in particular, as indicated by the red shaded area. For $m = 1$, this behavior is observed from the lowest frequency up to $St \approx 1.5$, whereas this difference is solely pronounced in the frequency range $0.2 \lesssim St \lesssim 1.5$ for $m = 0$. This prevalence of the leading mode is a strong indicator for a low-rank behavior of the jet.

RESOLVENT ANALYSIS

Optimal forcing and responses have been successfully computed for a range of flows in the past, such as channel flows (Jovanović & Bamieh, 2005), boundary layers (Monokrousos *et al.*, 2010; Sipp & Marquet, 2013), turbulent pipe flows (McKeon & Sharma, 2010; Sharma & McKeon, 2013; Gómez *et al.*, 2014), as well as incompressible

(Garnaud *et al.*, 2013) and compressible (Jeun *et al.*, 2016; Semeraro *et al.*, 2016) turbulent jets.

We start by noting that the full Navier-Stokes equations,

$$\frac{\partial q}{\partial t} = \mathcal{N}(q), \quad (6)$$

here written in symbolic notation where the operator $\mathcal{N}(q)$ represents their right-hand side, can be recast into a perturbation form

$$\frac{\partial q'}{\partial t} = \mathcal{A}q' + f, \quad (7)$$

by means of the Reynolds decomposition (1), and noting that $\frac{\partial q}{\partial t} = 0$. All terms linear in the perturbation state q' are lumped into the linear operator \mathcal{A} , and the remaining non-linear terms into the generic forcing function f . The spectral representation

$$(-i\omega - \mathcal{A}_m)q_{m\omega} = f_{m\omega}, \quad (8)$$

of equation (7) is obtained by assuming perturbations of normal mode form (2). We discretize equation (8) as

$$(-i\omega I - A_m)q_{m\omega} = Bf_{m\omega}, \quad (9)$$

where we introduced the forcing matrix B that allows us to restrict the forcing in space, or to specific quantities. Equation (10) can be written in compact form

$$q_{m\omega} = R_{m\omega}f_{m\omega}, \quad (10)$$

where we introduced the resolvent operator $R_{m\omega} = (-i\omega I - A_m)^{-1}B$ as the transfer function from forcings $f_{m\omega}$ to responses $q_{m\omega}$. Optimal forcings in terms of the energetic gain

$$\sigma^2(f_{m\omega}) = \frac{\langle q_{m\omega}, q_{m\omega} \rangle_E}{\langle f_{m\omega}, f_{m\omega} \rangle_E}, \quad (11)$$

can be computed as solutions to the eigenvalue problem

$$W^{-1}R_{m\omega}^H WR_{m\omega}\hat{f}_{m\omega}^{(i)} = \sigma_i^2 \hat{f}_{m\omega}^{(i)}. \quad (12)$$

with $\sigma_1 > \sigma_2 > \dots > \sigma^{(N)}$. The discretized eigenvalue problem (12) is solved using a standard IRAM method, yielding two orthonormal bases $\hat{F} = [\hat{f}_{m\omega}^{(1)} \ \hat{f}_{m\omega}^{(2)} \ \dots \ \hat{f}_{m\omega}^{(N)}]$ and $\hat{Q} = [\hat{q}_{m\omega}^{(1)} \ \hat{q}_{m\omega}^{(2)} \ \dots \ \hat{q}_{m\omega}^{(N)}]$ of optimal forcing and response vectors, respectively. In the present study, we discretize the LES solution domain $x, r \in [0, 30] \times [0, 6]$ with a 950×195 points Cartesian grid using the same numerical framework as in Schmidt *et al.* (2016a,c, 2017). Grid points are clustered in regions of high shear such as the shear-layer in the near-nozzle region. The domain size restricts the analysis to frequencies of $St \gtrsim 0.2$, below which

the forcing and response structures become too long to fit in the domain. The grid resolution imposes an upper limit of $St \approx 1.5$, above which the increasingly high wavenumbers cannot be resolved sufficiently.

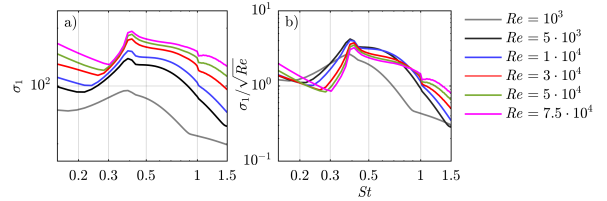


Figure 4. Optimal gain spectra for varying Reynolds numbers.

Figure 4 addresses the effect of the Reynolds number on the optimal gain for $m = 0$. The optimal gain monotonically increases with increasing Reynolds number, as can be seen in figure 4a, and all curves with $Re > 10^3$ approximately collapse under a $Re^{-1/2}$ scaling, as shown in figure 4b. The modal structures (not depicted) are found to agree well with the SPOD modes for $Re \geq 10^4$. At high Reynolds numbers $Re \geq 5 \cdot 10^4$, no further improvement of this agreement is observed, but the modal structures are increasingly hard to resolve, especially for suboptimals at higher frequencies. For these reasons, we chose an intermediate Reynolds number of $Re = 3 \cdot 10^4$ for the remainder of this study.

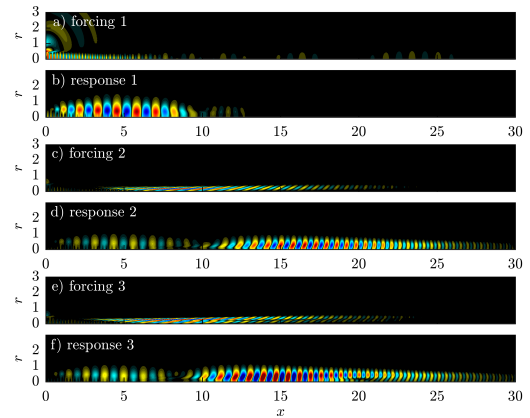


Figure 5. Pressure fields of the leading three optimal forcings and corresponding responses for $St = 0.5$ and $m = 0$.

Figure 5 shows the leading three optimal forcings and corresponding responses for $St = 0.5$ and $m = 0$, as an example. The leading response mode seen in figure 6b combines a compact K-H-type wavepacket with an acoustic core mode in the potential core. The response is forced by a combination of acoustic and vortical disturbances, predominantly acting in or on the initial shear layer and within the potential core, as can be seen in figure 6b. Please refer to Towne *et al.* (2016a) and Schmidt *et al.* (2016a) for details on the acoustic wave component. The two suboptimals exhibit a two-wavepacket structure with a larger spatial support, and are optimally forced in the shear layer downstream of the potential core.

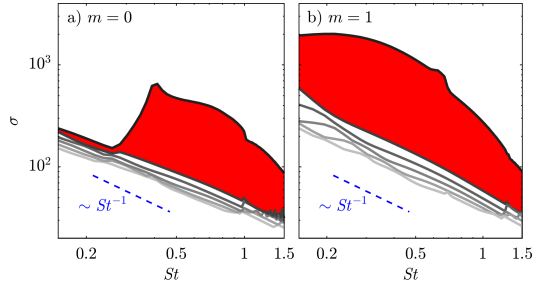


Figure 6. Resolvent gain (\blacksquare , $\sigma_1 > \sigma_2 > \dots > \sigma_N$) of the 6 leading modes as a function of frequency for $m = 0$ and $m = 1$. The difference between the leading and the second mode is highlighted in red (\blacksquare).

Resolvent gain spectra for $m = 0$ and $m = 1$ are depicted in figure 6. The highlighted areas (red) in both cases signify that the optimal gain curves are well separated from the first suboptimal and all subsequent gain curves over a range of frequencies. For $m = 0$, this behavior is cut on abruptly at $St \approx 0.2$, whereas it persists over the entire frequency range under consideration for $m = 1$. This dominance of the leading response mode was previously associated with the preferred amplification behavior observed in forced jets (Crow & Champagne, 1971) by Garnaud *et al.* (2013). It can also be seen that the suboptimal gain curves scale roughly as $\sigma \sim St^{-1}$, or as St^{-2} in terms of energy instead of gain. The same slope is shown in the SPOD spectra depicted in figure 3 above, for comparison.

OPTIMAL VS. EMPIRICAL RESULTS

In the preceding sections, we showed that leading empirical SPOD and optimal resolvent response modes both resemble K-H wavepackets. Furthermore, the SPOD analysis suggested that the natural jet at hand exhibits a low-rank behavior in accordance with the predictions of the resolvent analysis. The preferred amplification behavior of forced jets studied by (Crow & Champagne, 1971), presumably is a manifestation of exactly this low-rank behavior which we observe in a statistical sense in the natural jet at hand. In the following, we compare the empirical results to optimal linear theory in order to support this argument.

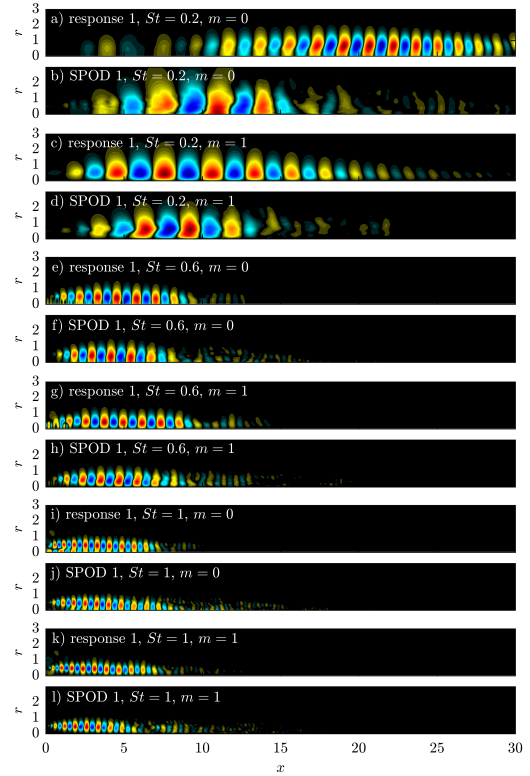


Figure 7. Optimal resolvent response modes and empirical SPOD modes for $m = 0$ and $m = 1$ at different frequencies.

Figure 7 compares the modal structures of the leading optimal response modes for $m = 0$ and $m = 1$ at different frequencies to the corresponding SPOD modes extracted from the LES. The leading symmetric ($m = 0$) response mode at the lowest frequency $St = 0.2$ shown in figure 7a does not resemble the corresponding SPOD mode in figure 7b in terms of spatial support and streamwise wavenumber. A much better correspondence is found for $m = 1$ and the same frequency in figure 7c and 7d, respectively. For all higher frequencies and both azimuthal wavenumbers, a very good agreement between the theoretical and the empirical modes is found. When comparing these findings with the gain curves depicted in figure 6, we observe that the major discrepancy between the modes at $St = 0.2$, $m = 0$ coincides with the region in which no low-rank behavior is predicted by theory.

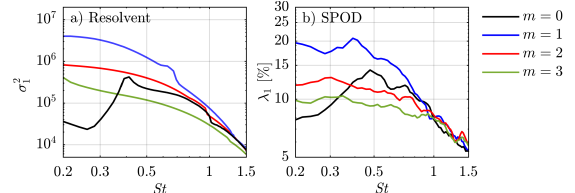


Figure 8. Leading optimal resolvent gains, and leading SPOD mode energies as a function of frequency for $m = 0, \dots, 3$.

We further investigate the low-rank behavior of the jet by comparing the optimal resolvent gain to the empirical modal energy content for different azimuthal wavenumbers

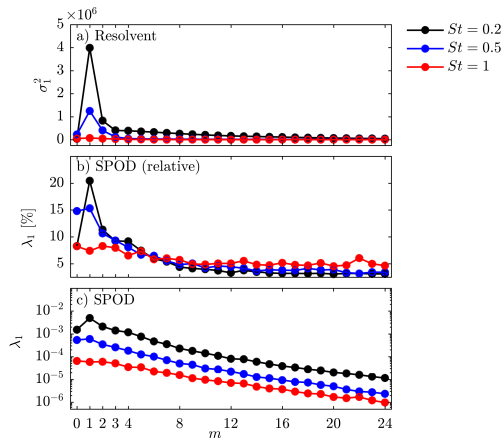


Figure 9. Leading optimal resolvent gains and SPOD mode energies for three representative frequencies as a function of m .

in figure 8. In 8b, the SPOD eigenvalues are normalized with respect to total energy at each given frequency. This allows for a direct comparison with the optimal resolvent gains, that are linear by construction and hence do not possess a physical amplitude that relates solutions at different frequencies. The SPOD eigenvalue curves have been smoothed using a five-point moving average for clarity. A good qualitative agreement is found between the optimal gains and the modal energies in terms of their relative order and frequency dependence. The leading $m = 1$ mode is dominant up to $St \approx 1$. The predicted abrupt change to low-rank behavior is clearly observed for $m = 0$. This finding explains the success of the near-field wavepacket models by Gudmundsson & Colonius (2011) and Cavalieri *et al.* (2013), but also sheds light on why the favorable agreement of their parabolized stability equation (PSE) solutions did not extend frequencies of $St \lesssim 0.3$ at $m = 0$. The dependence of the optimal gain and the empirical modal energy on the azimuthal wavenumber is studied in figure 9. As the jet is statistically stationary and round, we restrict our attention to the positive m sector, i.e. under the premise that the SPOD wavenumber spectrum is symmetric to a great degree. Three representative frequencies are picked as examples. For all azimuthal wavenumbers but $m = 0$, the leading mode of the lowest frequency of $St = 0.2$ dominates in the resolvent analysis in figure 9a. The higher gain of the $St = 0.5$ mode for $m = 0$ is another manifestation of the preferred amplification behavior as previously discussed in the context of figure 8. For $m < 5$, the general trend of increasing energy with decreasing frequency as predicted by the resolvent analysis is also reflected in the normalized SPOD mode energies plotted in 9b. The peak at $m = 1$ found in agreement in both graphs confirms that the prediction of a high optimal gain directly translates into higher modal energy levels in the actual flow. From 9c, it can be inferred that the modal structures at lower frequency are in general more energetic, which can be explained through the presence of an energy cascade, and the observation that the spacial support of the wavepackets decreases with frequency.

Acknowledgements OTS gratefully acknowledges support by DFG grant no. 3114/1-1. We acknowledge the support of the Office of Naval Research grant No. N00014-16-1-2445 with Dr. Knox Millsaps as program manager. The LES study was supported by NAVAIR SBIR

project, under the supervision of Dr. John T. Spyropoulos. The main LES calculations were carried out on CRAY XE6 machines at DoD HPC facilities in ERDC DSRC.

REFERENCES

- Brès, G. A., Ham, F. E., Nichols, J. W. & Lele, S. K. 2017 Unstructured large-eddy simulations of supersonic jets. *AIAA Journal* pp. 1–21.
- Cavalieri, A. V. G., Rodríguez, D., Jordan, P., Colonius, T. & Gervais, Y. 2013 Wavepackets in the velocity field of turbulent jets. *Journal of Fluid Mechanics* **730**, 559–592.
- Crighton, D. G. & Gaster, M. 1976 Stability of slowly diverging jet flow. *Journal of Fluid Mechanics* **77** (02), 397–413.
- Crow, S. C. & Champagne, F. H. 1971 Orderly structure in jet turbulence. *Journal of Fluid Mechanics* **48** (03), 547–591.
- Garnaud, X., Lesshafft, L., Schmid, P. J. & Huerre, P. 2013 The preferred mode of incompressible jets: linear frequency response analysis. *Journal of Fluid Mechanics* **716**, 189–202.
- Gómez, F., Blackburn, H. M., Rudman, M., McKeon, B. J., Luhar, M., Moarref, R. & Sharma, A. S. 2014 On the origin of frequency sparsity in direct numerical simulations of turbulent pipe flow. *Physics of Fluids* **26** (10), 101703.
- Gudmundsson, K. & Colonius, T. 2011 Instability wave models for the near-field fluctuations of turbulent jets. *Journal of Fluid Mechanics* **689**, 97–128.
- Jeun, J., Nichols, J. W. & Jovanović, M. R. 2016 Input-output analysis of high-speed axisymmetric isothermal jet noise. *Physics of Fluids (1994-present)* **28** (4), 047101.
- Jordan, P. & Colonius, T. 2013 Wave packets and turbulent jet noise. *Annual Review of Fluid Mechanics* **45**, 173–195.
- Jovanović, M. R. & Bamieh, B. 2005 Componentwise energy amplification in channel flows. *Journal of Fluid Mechanics* **534**, 145–183.
- McKeon, B. J. & Sharma, A. S. 2010 A critical-layer framework for turbulent pipe flow. *Journal of Fluid Mechanics* **658**, 336382.
- Mollo-Christensen, E. 1963 Measurements of near field pressure of subsonic jets. *Tech. Rep.*. Advis. Group Aeronaut. Res. Dev.
- Monokrousos, A., Åkervik, E., Brandt, L. & Henningson, D. S. 2010 Global three-dimensional optimal disturbances in the blasius boundary-layer flow using time-steppers. *Journal of Fluid Mechanics* **650**, 181–214.
- Schmidt, O. T., Colonius, T. & Brs, G. A. 2017 Wavepacket intermittency and its role in turbulent jet noise. In *AIAA Science and Technology Forum and Exposition (accepted)*. American Institute of Aeronautics and Astronautics (AIAA).
- Schmidt, O. T., Towne, A., Colonius, T., Cavalieri, A., Jordan, P. & Brès, G. A. 2016a Wavepackets and trapped acoustic modes in a mach 0.9 turbulent jet: a global stability analysis. *submitted to Journal of Fluid Mechanics*.
- Schmidt, O. T., Towne, A., Colonius, T., Jordan, P., Jaunet, V., Cavalieri, A. V. G. & Brès, G. A. 2016b Super- and multi-directive acoustic radiation by linear global modes of a turbulent jet. In *22nd AIAA/CEAS Aeroacoustics Conference*, p. 2808.
- Schmidt, O. T., Towne, A., Colonius, T., Jordan, P., Jaunet,

- V., Cavalieri, A. V. G. & Brès, G. A. 2016c Super- and multi-directive acoustic radiation by linear global modes of a turbulent jet. In *22nd AIAA/CEAS Aeroacoustics Conference*. American Institute of Aeronautics and Astronautics (AIAA).
- Semeraro, O., Lesshafft, L., Jaunet, V. & Jordan, P. 2016 Modeling of coherent structures in a turbulent jet as global linear instability wavepackets: Theory and experiment. *International Journal of Heat and Fluid Flow* **62**, 24–32.
- Sharma, A. S. & McKeon, B. J. 2013 On coherent structure in wall turbulence. *Journal of Fluid Mechanics* **728**, 196–238.
- Sipp, D. & Marquet, O. 2013 Characterization of noise amplifiers with global singular modes: the case of the leading-edge flat-plate boundary layer. *Theoretical and Computational Fluid Dynamics* **27** (5), 617–635.
- Towne, A., Cavalieri, A., Jordan, P., Colonius, T., Schmidt, O. T., Jaunet, V. & Brès, G. A. 2016a Trapped acoustic waves in the potential core of subsonic turbulent jets. *submitted to Journal of Fluid Mechanics* .
- Towne, A., Cavalieri, A. V. G., Jordan, P., Colonius, T., Jaunet, V., Schmidt, O. T. & Brès, G. A. 2016b Trapped acoustic waves in the potential core of subsonic jets. In *22nd AIAA/CEAS Aeroacoustics Conference*, p. 2809.